



Publication Year	2020
Acceptance in OA@INAF	2021-12-09T15:36:42Z
Title	X-ray absorption in INTEGRAL AGN: Host galaxy inclination
Authors	MALIZIA, ANGELA; BASSANI, LOREDANA; STEPHEN, JOHN BUCHAN; BAZZANO, ANGELA; P. Ubertini
DOI	10.1051/0004-6361/202038014
Handle	http://hdl.handle.net/20.500.12386/31211
Journal	ASTRONOMY & ASTROPHYSICS
Number	639

X-ray absorption in INTEGRAL AGN: Host galaxy inclination

A. Malizia,¹ L. Bassani,¹ J. B. Stephen,¹ A. Bazzano² and P. Ubertini²

¹ OAS-IASF-Bologna, Via P. Gobetti 101, I-40129 Bologna, Italy

e-mail: angela.malizia@inaf.it

² IAPS-IASF-Roma, Via Fosso del Cavaliere 100, I-00133, Roma, Italy

Received ; accepted

ABSTRACT

In this work the INTEGRAL hard X-ray selected sample of AGN has been used to investigate the possible contribution of absorbing material distributed within the host galaxies to the total amount of N_H measured in the X-ray band. We collected all the available axial ratio measurements of the galaxies hosting our AGN together with their morphological information and find that also for our hard X-ray selected sample a deficit of edge-on galaxies hosting type 1 AGN is present. We estimate that in our hard X-ray selected sample there is a deficit of 24% ($\pm 5\%$) of type 1 AGN. Possible bias in redshift has been excluded, as we found the same effect in a well determined range of z where the number and the distributions of the two classes are statistically the same. Our findings clearly indicate that material located in the host galaxy on scales of hundreds of parsecs and not aligned with the putative absorbing torus of the AGN can contribute to the total amount of column density. This galactic absorber can be large enough to hide the broad line region of some type 1 AGN causing their classification as type 2 objects and giving rise to the deficiency of type 1 in edge-on galaxies.

Key words. X-rays: galaxies – galaxies: active – galaxies: Seyfert

1. Introduction

The nature of the absorbing material hiding the central engine of active galactic nuclei (AGN) is crucial to our understanding of the physics of these objects (Hickox & Alexander 2018). It is also a key issue in the unified model of AGN (Antonucci 1993; Urry & Padovani 1995) which in its simplest version postulates that the diversity of AGN can be largely explained as a viewing angle effect. The most important ingredient of this orientation-based model is an optically and geometrically thick torus that obscures the nuclear regions of an active galaxy (the accretion disk and the hot corona as well as the broad line region (BLR)). We optically classify an AGN as type 2 or type 1 depending if our line of sight intercepts or not the obscuring material of the torus.

The validity of the unified model of AGN has largely been tested and confirmed by the presence of high absorption measured in the X-ray spectra of type 2 with respect to lower amounts found in type 1 AGN. In particular, using a sample of 272 AGN observed at high energies (> 20 keV) by INTEGRAL/IBIS we have found that the standard-based AGN unification scheme is followed by the majority of bright AGN (Malizia et al. 2012) with only a few exceptions related to 12–13% of the objects. These exceptions are absorbed type 1 and unabsorbed type 2 AGN. The absorption in type 1 AGN is generally interpreted in terms of ionised gas located in an accretion disc wind or in the biconical structure associated with the

central nucleus and therefore unrelated to the torus. The lack of X-ray absorption ($N_H < 10^{22} \text{ cm}^{-2}$) in type 2 AGN could be explained by the assumption that the torus is either not present (or has disappeared) or the source has been misclassified. The first case is probably true for low luminosity objects (Elitzur 2008) while the second case is relevant for the class of intermediate type 2 Seyfert (type 1.8 – 1.9). These intermediate objects have historically been considered as AGN where the observer’s line of sight intercepts either the outer edge of the torus or a limited number of clouds, so that the broad line region is still partly visible. However, in Malizia et al. (2012) we have also pointed out that these intermediate classifications can be explained by an intrinsically variable ionising continuum or by the presence of absorption/reddening unrelated to the torus. For example, a source that would normally appear as a type 1 Seyfert can be classified as an intermediate type if it is in a low optical flux state (Trippe et al. 2010) or if its BLR is obscured (except for the strongest H_α line) by dust related to large-scale structures such as bars, dust lanes and host galaxy material (Malkan et al. 1998; Matt 2000).

Thus absorption in AGN is probably due not only to one component, the torus, but to multiple components on very different scales. Bianchi et al. (2012) identified 3 such components: the BLR on the 0.01 pc scale, the torus on a parsec scale and absorption located in the host galaxy on a scale of hundreds of parsecs.

Evidence for large scale absorption comes mostly from

inclination studies of the host galaxies of AGN. In one of the first such studies Keel (1980) found that optically-selected (mostly type 1) Seyferts tend to avoid edge-on host galaxies. Using a sample of AGN selected in the soft X-ray band (0.2-3.5 keV), Simcoe et al. (1997) subsequently confirmed the bias against edge-on Seyfert 1 although they were able to recover some of the edge-on AGN missed in UV and visible surveys, resulting in 30% incompleteness for type 1's. However since the soft X-ray band can also be biased in terms of absorption, a definitive test would be provided by the use of a hard X-ray selected sample. A preliminary analysis performed on a Swift/BAT sample of around 80 AGN by Winter et al. (2009) showed that objects with low X-ray column densities were preferentially found in galaxies with low inclination angles (face-on, $b/a > 0.5$), while those with higher column densities were found in galaxies of any inclination (edge-on and face-on, $0.1 < b/a < 1$). The finding that optically selected AGN samples tend to avoid edge-on systems, has recently been confirmed and refined with much higher statistics by using the SDSS survey (Lagos et al. 2011).

The first explanations for this result came from Maiolino & Rieke (1995) and Matt (2000). Maiolino & Rieke (1995) proposed the *dual absorber* model which foresees the existence of a 100 pc scale obscuring material of molecular gas coplanar with the galactic disc and not necessarily aligned with the torus. On the other hand, taking into account observational evidence, Matt (2000) proposed a scenario where Compton thick Seyfert 2 galaxies are those sources observed through the torus while Compton thin/intermediate Seyfert galaxies are obscured by dust lanes at larger distances.

Focusing on the possible origin of the galactic absorber, a major study is that of Malkan et al. (1998), who detected fine-scale structure in the centres of nearby galaxies using HST images: these structures include dust lanes and patches, bars, rings, wisps, filaments and tidal features such as warps and tails. These authors even suggested a new unified model (the galactic dust model) whereby the obscuration that converts an intrinsic Seyfert 1 nucleus into an apparent Seyfert 2 occurs in the host galaxy hundreds of parsecs from the nucleus. More recently Prieto et al. (2014) confirmed these early results of large scale, a few hundred pc, dust filaments and diffuse dust lanes hiding the central region of some AGN.

Nowadays the parsec scale environment of AGN can be spatially resolved by high angular resolution observations in the infrared (IR) with VLTI and in the sub-Millimeter by ALMA (see e.g. Höning & Kishimoto (2017); Combes et al. (2019)) which draws a much more complex picture of multi-phase and multi-component regions. Recently Höning (2019) has proposed a model which accounts for these new observations wherein dusty molecular gas flows in from the host galaxy (~ 100 pc) to the sub-parsec environment via a disc with small to moderate height. Due to the radiation pressure, the disc puffs up and unbinds a large amount of the inflowing gas from the black hole's gravitational potential allowing the creation of dusty molecular winds driven by the radiation pressure from the AGN. These dusty winds feed back the host galaxy with a rate increasing with the AGN luminosity (or Eddington ratio), and are therefore a mechanism to self-regulate the AGN activity providing a feedback from AGN to host galaxy. Within this picture there are multiple spatial and dynamical

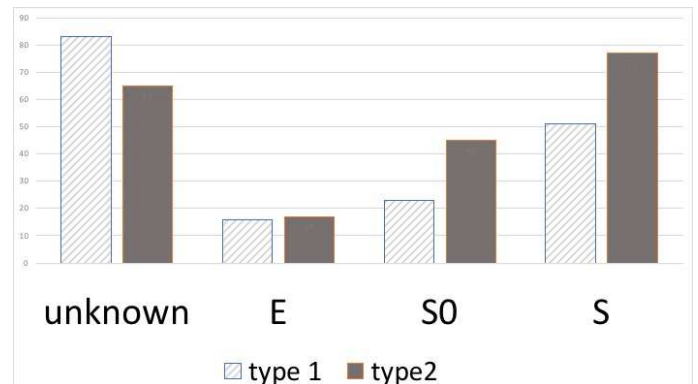


Fig. 1. Histogram of the morphological classification following the de Vaucouleurs (1959) scheme. Unknown: galaxies which have no host galaxy morphology, E: elliptical galaxies; S0: intermediate systems between ellipticals and spirals; S: spiral galaxies. Objects are further sub-divided in type 1 and type 2.

components which obscure the primary emission rather than a single torus. For local, radio quiet active galaxies, Hoenig's model is consistent with the structure proposed by Ricci et al. (2017) to explain the X-ray obscuration in AGN. ALMA observations have revealed the presence of circumnuclear molecular (CO) gas in many Seyfert galaxies (Schinnerer et al. 1999), as well as the presence of cold gas and dust at hundreds of pc scales in many AGN host galaxies (e.g. García-Burillo et al. 2005, 2014).

Finally, we note that large scale absorption may come also from non asymmetric perturbations which provide a viable way to channel gas from the outer part of a galaxy into its central regions. These perturbations can be of two types: external, such as galaxy-galaxy interactions or internal, such as due to bars and their gravity torques. Observations indicate that an AGN becomes heavily obscured behind merger-driven gas and dust, even in the early stages of galaxy-galaxy interaction, when the galaxies are still well separated (Kocevski et al. 2015). Furthermore, analysis of Swift/BAT AGN indicates that a large fraction (25%) of these objects show disturbed morphologies or are in close physical pairs compared to matched control galaxies or optically selected AGN (Koss et al. 2010).

In this paper we will investigate the presence/role of obscuration on large galactic scales and its relation with the X-ray column density, by examining the axial ratio distribution in a well defined sample of INTEGRAL selected AGN, listed in Malizia et al. (2012, 2016) and newly reported in this work. This sample, being hard X-ray selected, is the most appropriate to carry out this type of study since it is unbiased against obscured objects and therefore free of the limitation which affects surveys at other frequencies (i.e. from optical to soft X-rays).

2. The sample

In order to have a well defined hard X-ray selected sample of active galactic nuclei, we have considered all the INTEGRAL Seyferts listed in Malizia et al. (2012, 2016) plus those reported in Tables A.2 and A.3 of the Appendix. This hard X-ray selected sample of AGN has been extracted from the INTEGRAL/IBIS all sky surveys performed so far in the 20-100 keV band (Bird et al. (2016) and reference therein). This sample has been updated in

this work with the addition of the new AGN reported by Mereminskiy et al. (2016) in the deep extragalactic surveys of M81, LMC and 3C 273/Coma regions and those reported by Krivonos et al. (2017) in the Galactic Plane Survey (see Appendix and Tables A.2 and A.3 for details on these new additions).

The entire INTEGRAL AGN sample is fully characterised in terms of optical identification/classification and is also fully studied in terms of X-ray spectral properties (see Malizia et al. (2012)). In particular, the column densities (N_H) measured in the 2-10 keV band for each AGN, have been collected from the literature (see Malizia et al. (2012, 2016)) or calculated for the new added sources in this work (see Appendix, Tables A.2 and A.3). All together, we have gathered a sample of 376 hard X-ray selected active galaxies, with a well defined set of information. Objects identified as Blazars in the IBIS surveys have been excluded from the analysis to avoid complication due to the presence of jets pointing towards the observer. Following our previous works we divided our AGN into type 1 comprising all the broad line Seyferts of our sample and including Seyfert 1, 1.2, 1.5 (179 objects) and type 2 objects comprising all the narrow line AGN i.e. Seyfert 1.8, 1.9 and 2 (197 objects). Twenty-two objects ($\sim 6\%$ of the sample) have an unknown optical classification or belong to non-Seyfert optical classes (liners, XBONG, AGN), therefore they have been assimilated into type 1 or 2 AGN depending if they were absorbed (21 objects) or not in the X-ray band. Performing the complete analysis without these sources does not significantly change the overall results.

In order to investigate the role of absorption in the host galaxy we have collected for the entire sample the axial ratio b/a , used here as a proxy for the host galaxy inclination (to first order, $\cos i = b/a$ where a and b are the observed major and minor axes of a galaxy and i is its inclination). These values have been collected from the Two Micron All Sky Survey¹, where information was available for 300 objects out of 376 in the sample (i.e. the largest coverage available in catalogues with b/a informations) and they are reported in columns 5 and 10 of tables A.1 and A.2/A.3 respectively. It is worth noting that as described by Jarrett et al. (2003), the 2MASS images, co-adding J, H and K bands, have a point spread function FWHM of 2 - 3 arcsec. This value is much smaller than the radii of our galaxies (around 20-30 arcsec or more) collected from the same archive, therefore excluding any possible bias in the b/a measurements used in our work, especially for type 1 objects hosting a bright nucleus. Furthermore, in order to verify the accuracy of these axial ratios, we have used Pan-STARRS1 database (Chambers et al. 2016) and extracted the DR1 color (g to z filter) images for a representative sample of over 30 of our objects ranging in axial ratio from 0.1 to 0.9 and over all optical classes. Representative set of objects among those with no optical classification has also been checked. We then fitted ellipses to these images in order to measure their axial ratio values. In every case these values were consistent with those extracted from the 2MASS surveys and originally used.

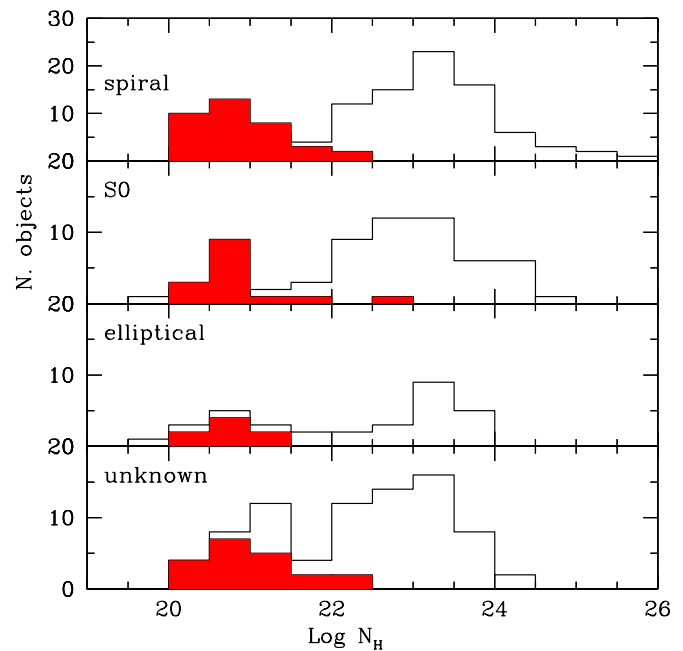


Fig. 2. Distribution of column density in each morphological class; X-ray absorption in AGN hosted in galaxies of unknown class is also shown. Filled red bins referred to Galactic or upper limit values of N_H .

3. Absorption and source morphology

Indications that absorption on a galaxy scale is important in the overall column density budget of an AGN, suggests a possible link between galaxy morphology and N_H . We have therefore collected data for both these two parameters. Data for host galaxy morphological information for all objects come from the Hyperleda catalogue (Makarov et al. 2014), the NED archive and the 2MASS Redshift Survey (Huchra et al. 2012): the most quoted classification among these 3 databases has been adopted and reported in tables A1, A2 and A3. When no information or different classification were available, we have also searched the literature for extra information (Maiolino et al. 1999, Madrid et al. 2006, McKernan et al. 2010, Maia et al. 2003, Tsvetanov et al. 1992 and Ferruit et al. 2000). Data for N_H values comes instead from our previous publications and current paper as specified in section 2.

All the INTEGRAL AGN have been divided into 3 broad morphological types following the de Vaucouleurs (1959) scheme: E to describe elliptical galaxies; S0 for objects which are intermediate systems between ellipticals and spirals (alternatively called lenticular galaxies), and S for spiral galaxies. The distribution of INTEGRAL AGN in each morphological class, including those objects for which the host galaxy morphology is unknown, is shown in figure 1, where the predominance of spiral/lenticular galaxies over ellipticals is evident. The greater number of type 2 over type 1 AGN in both S0 and S classes is also clear.

We have been able to obtain morphological host galaxy information for 228 objects or 61% of the sample. This low fraction is due to the fact that many INTEGRAL AGN are newly discovered galaxies, often located on the Galactic Plane, i.e. in the zone of avoidance and therefore their morphology is still poorly studied. In the nearby Uni-

¹ <http://irsa.ipac.caltech.edu/cgi-bin/Gator/nph-dd>

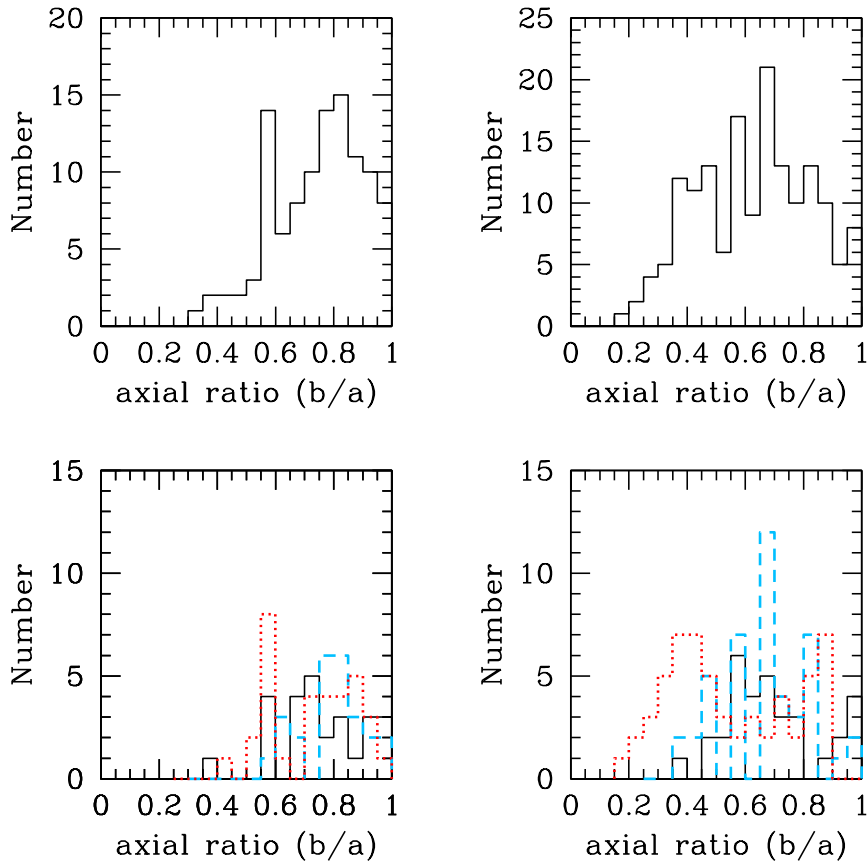


Fig. 3. Distribution of host galaxy axial ratios of INTEGRAL AGN differentiated into broad lines or type 1 i.e. Sy 1 - 1.2 - 1.5 (upper and lower left panels) and narrow lines or type 2 i.e. Sy 1.8 - 1.9 - 2 (upper and lower right panels). In the lower panels the morphological type of our sample sources has been considered; histograms in dotted red lines refer to AGN hosted in late type (Spirals) galaxies, blue dashed lines AGN hosted in early (Elliptical and S0) galaxies and black solid lines refer to host galaxies for which no morphological type has been found in the literature.

verse, elliptical galaxies are known to have less gas, dust, and ongoing star formation activity than spiral galaxies (Hirashita & Nozawa (2017) and references therein). Figure 2 shows the histogram of each morphological class as a function of X-ray column density: while there seem to be no difference in absorption properties among different classes for column density below $\text{Log}N_H = 24$, some difference is evident above, since no Compton thick AGN is hosted in an elliptical host galaxy. However, this may be due to low number statistics, given the limited number of ellipticals considered here as they count for only 14% of the entire INTEGRAL AGN sample. The fraction of heavily absorbed AGN is around 11% for both spiral and lenticular galaxies; if the same fraction is applied to ellipticals, then we would expect 3-4 objects in this class to be Compton thick, while none is observed.

The evidence of a lower fraction of Compton thick AGN in hard X-ray radio galaxies, typically hosted in elliptical galaxies, has already been discussed by Panessa et al. (2016) and Ursini et al. (2017) and is definitely an issue that deserves further investigation. Ursini et al. (2017) also noted that a significant role in the absorption of heavily absorbed radio galaxies could be played by material different from the classical pc-scale torus such as that traced by 21 cm H_I absorption, which can be located much farther away, e.g. at galactic scales. Hence observational evidence

even questions the origin of the X-ray absorption in ellipticals and hints at a possible difference between the average properties of ellipticals compared to lenticular/spiral galaxies, especially in terms of Compton thick absorption.

4. Host galaxies inclination

Using the large INTEGRAL AGN sample, we explore in this section the axial ratio distribution of broad and narrow line AGN: figure 3 displays the histograms of b/a by galaxy type and within each type divided in morphological classes. Note that the lack of galaxies with $b/a < 0.2$ is due to the non zero thickness of the disc which accounts for the fact that, even when seen edge-on, a galaxy has b/a greater than zero (Hubble 1926). Among the 122 type 1 AGN of our sample for which we obtained axial ratio information, only 12 (<10%) have a host galaxy axial ratio below 0.5; this percentage is much higher in type 2 AGN where 50 out of 178 type 2 objects (or 28%) have $b/a < 0.5$ ². By performing a KS test, we find that the axial ratio distributions of type 1 and type 2 AGN are different, since the probability

² It is worth noting that the absorbed sources with no optical class considered as type 2, have axial ratio distributed over the whole range of b/a , and the only unclassified source included in the type 1 class, has $b/a = 0.58$.

that the two samples come from the same distribution is rejected at a confidence level of 99.99%. In order to quantify the deficit of type 1 AGN at low inclination angles, we compare the two histogram distributions. Taking the difference between the two histograms, and assuming that above an inclination angle of 0.5 they are from identical distributions, we normalise it so that the total difference in number of sources above that value is zero. In order to have a difference of zero below that threshold, 38 ± 11 sources must be missing from the type 1 distribution. This implies that in this sample there is a deficit of about 24% ($\pm 5\%$) of type 1 AGN, in agreement with Simcoe et al. (1997) who found 30% for an X-ray selected sample.

Furthermore, using the information on the host galaxies morphology and dividing the objects into early (Ellipticals and S0) and late (Spirals) types, we also checked if the bias against edge-on host galaxies of broad line AGN is related to any specific morphological type or is present in both types. Using (here and in the following) a confidence level of 99% and applying the KS test, we find that the two distributions (type 1 versus type 2 AGN) are different both for early type as well as late type objects. This is also evident in figure 3 where the different morphology types have been highlighted for type 1 and 2 AGN respectively. We therefore confirm that, even using AGN selected above 20 keV, the deficit of type 1 AGN hosted in edge-on galaxies exists in, and is independent of, all morphological types.

In addition to this deficit, it is interesting that the type 2 are distributed over the whole range of b/a . This result confirms previous findings but also highlights the fact that this lack of Seyfert 1 in edge-on galaxies is not due to observational bias. As pointed out by Gelbord et al. (2006), if the torus was the only obscuration matter, then two possible scenarios should be taken into consideration: the first where the torus and the host galaxy plane are aligned and the second where the two are misaligned. In the first case we should see a distribution of type 1 Seyferts peaked in face-on galaxies and that of the type 2 Seyferts in edge-on galaxies while in the second case no correlation between Seyfert type and host galaxy inclination would be expected. From the studies performed so far and confirmed herein, neither of these two scenarios are compatible with the observational evidence since the broad line AGN have a strong correlation with the host inclination angle while the type 2 are broadly distributed over the whole b/a range. Our findings indicate that something intervenes outside the nucleus of the AGN (on hundreds of pc scales), likely in the host galaxy; this absorbing material, which could be not aligned with the torus, can contribute to the final column density measured in the X-ray band.

From recent ALMA observations of some AGN, we have an indication that the molecular discs, or tori, detected at 10 pc scales are kinematically decoupled from their host galaxy disc and have random orientations (Combes et al. 2019). Assuming a simplistic approach, i.e. not considering the BLR but only the host galaxy and the torus, depending on their relative alignment or misalignment we expect the following 4 configurations. If the torus is edge-on, the source is always classified as a type 2 AGN and should present X-ray absorption, whether or not the galaxy is seen edge-on or face-on. If the torus is seen face-on, then we should expect a type 1 AGN configuration with no or very mild absorption unless the galaxy is seen edge-on and has absorbing material on large scale. In this last case the source could

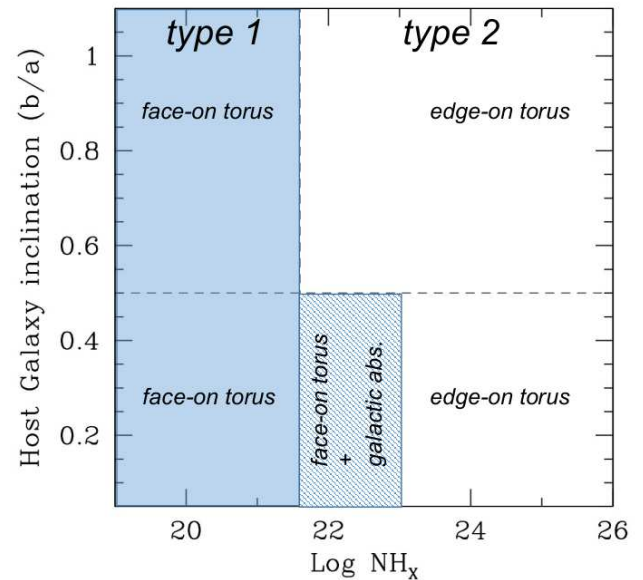


Fig. 4. Scheme of the expected type of absorption in the b/a - $\log N_H$ plane for broad line (left blue side) and narrow line AGN (right side) in relation to the torus/host galaxy misalignment. The dashed blue region represents values where a possible type 1 AGN could be classified as type 2 due to absorption located in the host galaxy.

be wrongly classified as a type 2 AGN although the absorption is not related to the torus. This is schematically shown in figure 4 where the horizontal line represents the dividing line between face-on and edge-on host galaxies at $b/a = 0.5$, while the first vertical line represents instead the value of $N_H = 4 \times 10^{21} \text{ cm}^{-2}$ which has been assumed as the dividing line between absorbed/unabsorbed objects. This value has been taken from Mateos et al. (2016) and corresponds to the extinction level capable of hiding the BLR. The dashed region delimited by $\log N_H \leq 23$ and $b/a \leq 0.5$, represents the area where misclassified type 1 AGN could be located (i.e. galaxy absorption in an edge-on host is sufficient to hide the broad line region). With this scheme in mind, we can now investigate the relation between host galaxy inclination and X-ray absorption.

4.1. Possible bias on redshift

Before drawing any further conclusions from the observed axial ratio distribution, any possible bias introduced by the sample redshift distribution must be checked. It is important to investigate this issue since there are two considerations that pertain to the use of a non complete sample of AGN. The first is that at high redshifts, the sources become point-like and therefore it is very difficult to estimate the host galaxy axial ratio. The second concerns the widely known fact that in the local Universe type 2 objects outnumber type 1 sources by a factor of ~ 4 and more (Sazonov et al. 2015); whether this effect comes from cosmological reasons or not is still matter of debate. These two effects are highlighted in figure 5 where it is clear that the distributions of type 1 and type 2 galaxies are different in

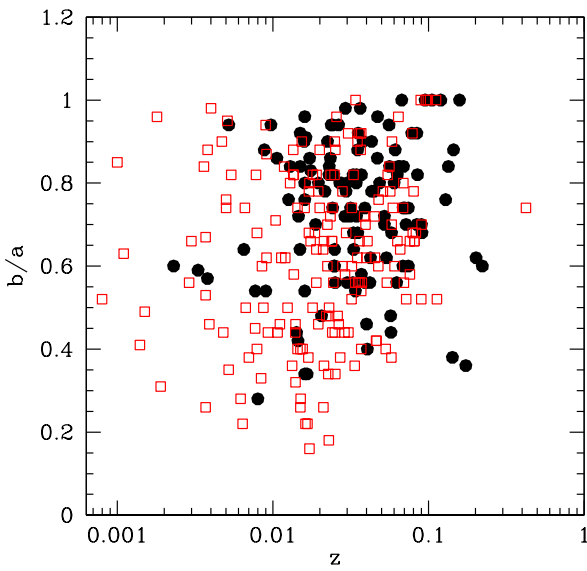


Fig. 5. Redshift values of the INTEGRAL AGN plotted against the axial ratios of their host galaxies. Filled black circles are type 1 AGN while open red squares are type 2.

the $z - b/a$ plane: there are considerably more type 2 AGN at low z values than type 1 and very few objects at high redshifts have axial ratio measurements. In order to minimise these effects, we have decided to analyse a subset of the two AGN populations restricting both high and low z values. To do this, we first choose all sources between a lower and higher limit of redshift. The distribution of type 1 and type 2 objects between these two limits are then compared and the KS statistic applied to identify if they come from the same population. This is done for all possible combinations of the two limits in z . The combination which provides the highest probability that the two populations come from the same z distribution (at 99.9% confidence) are then further reduced to give the largest total number of objects. In this manner, we found that allowing the redshift to range from 0.026 to 0.095, we obtained a total number of 133 AGN with z within this range; of these AGN, 66 are of type 1 and 67 of type 2, with a probability of 99.97% that they come from the same overall redshift distribution (top panels of figure 6). Next, the distribution of the axial ratio of these 133 sources divided in two optical classes were compared as shown in figure 6 (lower panels). Again the two distributions are found to be different, with type 1 objects mainly located in face-on galaxies and type 2 spread over the entire range of b/a values. Using the KS statistic we find that the likelihood that the two populations come from the same distribution is rejected at a confidence level of 99.75% implying that no bias in redshift affects our result.

5. Host galaxy inclination versus X-ray absorption

In order to investigate the deficit of type 1 AGN in edge-on galaxies in more detail, we first considered for each AGN type their optical sub-classes which is a way to investigate if and how the broad line region is detected. In figure 7 panel

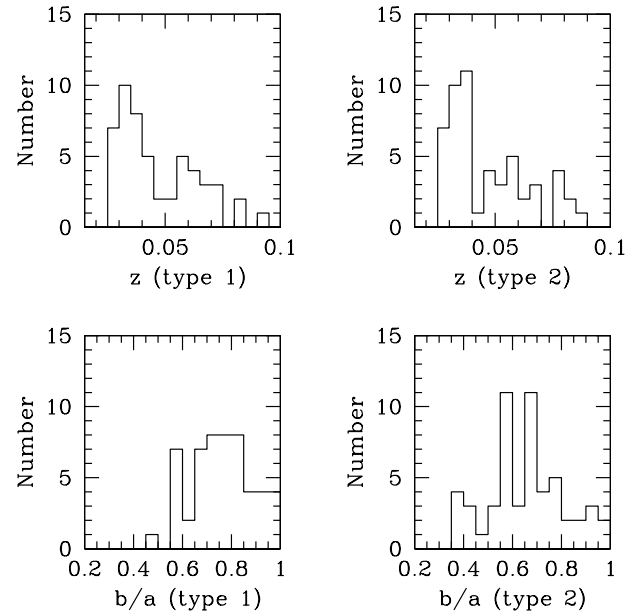


Fig. 6. In the upper panels the distributions of redshift values in type 1 (left) and type 2 (right) in the bin 0.026 and 0.095, while in the bottom panels the distributions of their relative axial ratios.

a), we compare the axial ratio distribution of Seyfert 1-1.2 (solid black line) and Seyfert 1.5 (dashed red line). As is evident in the figure but also quantified by the KS test, the two distributions are similar (at a confidence level of 99%) indicating that the deficit of broad line AGN in edge-on galaxies is present in all subclasses.

Equally, in panel b) of figure 7, the distribution of axial ratios in Seyfert 2 (black solid line) and Seyfert 1.8-1.9 (blue dashed line) are plotted in order to see if they are distributed differently and, as is clear from the histograms and quantified by the KS statistics, they are not. Also including all the sources of intermediate class (1.2, 1.5, 1.8 and 1.9) in the type 1 sample and leaving in the type 2 only the pure Seyfert 2 objects, the two distributions resulted statistically different. The same result has been found considering only the high energy selected AGN belonging to the INTEGRAL complete sample (Malizia et al. 2009).

In figure 7 panel c) we plot the axial ratios of type 1 AGN (Seyfert 1-1.2 black circles and Seyfert 1.5 red circles) versus the X-ray absorption, the open circles indicate no intrinsic absorption (i.e. only Galactic) or upper limits. Note that in panels c) and d) of figure 7 the horizontal and vertical dashed lines follow the scheme introduced in figure 4.

As expected from the scheme of figure 4, type 1 AGN fall mostly in the left, top side of panel c), i.e. correspond to the situation where the torus and the galaxy are both seen face-on and no or mild X-ray absorption is present. Regarding those type 1 AGN which, despite having torus and galaxy both face-on, display X-ray absorption (i.e. fall in the right upper side of panel c)) we assume that they can be largely explained as objects where the absorbing material is due to ionised gas located in accretion disc winds or in biconical structures close to the nucleus (Malizia et al. 2012). A more complex interpretation pertain to those type 1 AGN which are hosted in edge-on galaxies and therefore fall in

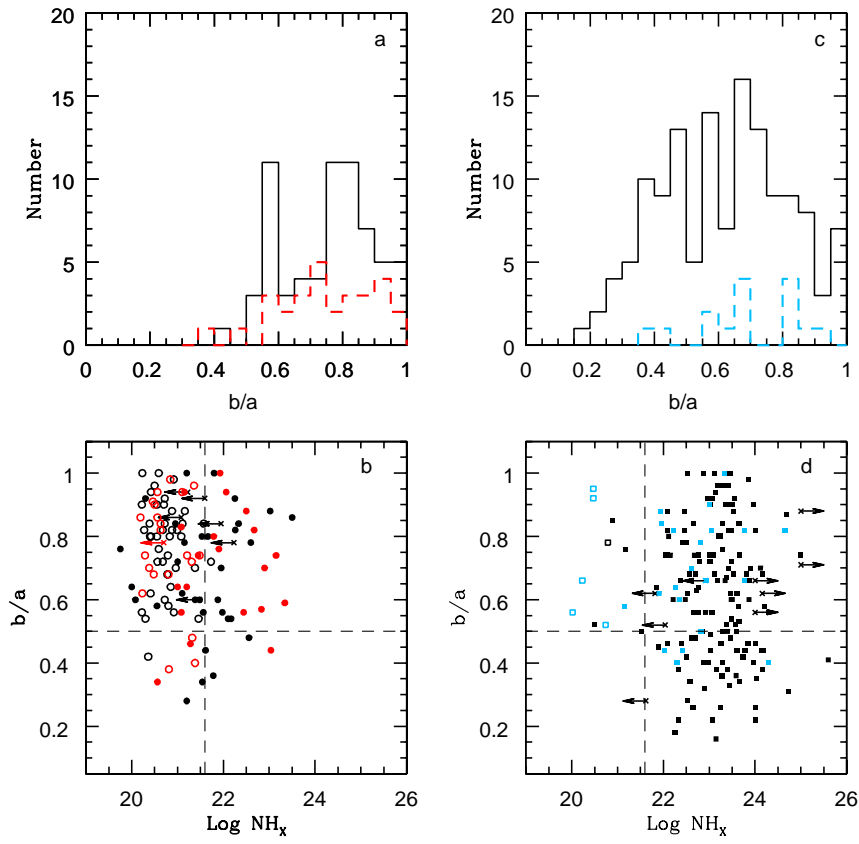


Fig. 7. Upper panels: distribution of host galaxy axial ratios. Panel a) Seyfert 1/1.2 (black line) and intermediate Seyfert 1.5 (red dashed line); panel b): Seyfert 2 (black line) and intermediate Seyfert 1.8/1.9 (blue dashed line). Lower panels: axial ratios versus X-ray absorption: c) broad line AGN (black circles Seyfert 1/1.2 and red circles Seyfert 1.5; panel d) narrow line AGN, black squares Seyfert 2 and blue squares Seyfert 1.8/1.9. Open circles refer to N_H upper limits or objects with no intrinsic absorption, i.e. only Galactic. Lines are like in figure 4.

the bottom parts of panel c). First we notice that their number is limited as expected on the basis of the consideration made in section 4. These low numbers can either be due to a low probability of having a configuration with a face-on torus in an edge-on galaxy or a high probability that absorbing material in a host galaxy viewed edge-on is sufficient to hide the BLR and to misclassify the object as a type 2 AGN. Since there is no reason why each of these possibilities is likely, it is possible that both concur to create the observed low number of type 1 AGN seen in edge-on galaxies. In particular we already know of type 1 AGN with absorbing material hosted in edge-on galaxies, which is however not high enough to hide the BLR. These are the objects located in the bottom left part of panel c); one of these AGN is IC 4329A where the presence of a dust lane observed in the equatorial plane of the host galaxy has been invoked to explain the source's mild X-ray neutral absorption which is however below our limit of $N_H = 4 \times 10^{21} \text{ cm}^{-2}$ (Steenbrugge et al. 2005). The most particular objects are the 3 AGN, IGR J05347-6015, 4C +21.55 and ESO 140-G43, in the bottom right corner of the panel c). Although they have a column density $\text{Log } N_H > 21.6$ and are hosted in low inclination angle galaxies, we still see their BLR. However, these objects are either poorly studied as in the case of IGR J05347-6015 and 4C +21.55 (only Swift-XRT short observations were available to estimate the

X-ray column density) or found to be absorbed by complex and ionised gas as for ESO 140-G43 (Ricci et al. 2010). In any case given the uncertainty on the column density of these 3 objects, and given their proximity to the chosen b/a and $\text{Log } N_H$ boundaries, no firm conclusion can be drawn. In panel d) of figure 7, the X-ray column density is plotted against the axial ratio of Seyfert 2 (black squares) and Seyfert 1.8-1.9 (blue squares) and, as for the type 1 AGN, open symbols indicate no intrinsic absorption or upper limits. In these objects the torus is by definition seen edge-on independently if the AGN is hosted in a face-on or an edge-on galaxy and their absorption is high: hence these objects are expected to spread on the right side of the diagram over all values of b/a . Here the unusual objects are those found in the upper left corner of panel d), which have a column density too low to completely hide the BLR. Not considering Sey1.8-1.9 types where an intrinsically variable ionising continuum or absorption/redening unrelated to the torus can explain their intermediate classification, there are 4 objects: NGC 4736, IGR J19260+4136, IGR J03249+4041-SW and IGR J14515-5542, optically classified as Seyfert 2, which have no absorption in X-rays. NGC 4736 is a nearby star-forming ring galaxy (van der Laan et al. 2015) where the torus is probably not present due to the low luminosity of the nucleus; star formation could then be responsible for the type 2 op-

tical class. IGR J03249+4041-SW is one component of a pair of Seyfert 2 in close interaction (pair distance around 12 Kpc) and it is therefore possible that its type 2 class is simply due to dust associated to the galaxy merging. The other two AGN are poorly studied, but their column density is well measured and confirmed using XMM-INTEGRAL data for IGR J14515-5542 (De Rosa et al. 2012) and NuSTAR data for IGR J19260+4136 (our analysis) respectively. The fact that no prominent iron line is seen at soft X-ray energies excludes that these are Compton thick AGN (see Malizia et al. 2007); it is therefore very likely that they belong to the small fraction of naked Seyfert 2 galaxies where the torus is missing and the optical classification is due to other circumstances (Panessa & Bassani 2002). Otherwise they can be type 1 AGN where the combined effect of a very broadened emission profile and an intrinsic weakness with respect to the host galaxy conspire to produce a type 2 spectrum (Bianchi et al. 2019).

The objects in the bottom right corner of panel d) are the most relevant for the aim of this work. Following the scheme of figure 4, for these type 2 objects we cannot discriminate between absorption due to material located on large scales and related to the host galaxy, and that due to the torus.

6. Discussion

It is a well known effect that optically selected type 1 Seyfert tend to avoid edge-on host galaxies. Extensive studies have been performed in different wavebands in order to explain this bias (Keel 1980; Simcoe et al. 1997; Lagos et al. 2011) and although some objects missed in UV and optical surveys have been recovered going at higher energies, the deficit of type 1 hosted in edge-on galaxies still remains. A definitive test is that provided by the use of a hard X-ray selected sample which is less biased against obscured objects and therefore free of the limitation which affects surveys at other frequencies (i.e. from optical to soft X-rays). The first test at high energies was performed by Winter et al. (2009) on a limited Swift/BAT sample of around 80 AGN and also with this selection, they found that edge-on galaxies only host the more absorbed AGN, finding that from the 11 edge-on sources in their sample, only one is associated with a Sey 1.

In this work using the INTEGRAL high energy selected sample of AGN (376 Seyferts), we have confirmed that there is a deficit of around 24% ($\pm 5\%$) of type 1 objects hosted in edge-on galaxies. Since this bias is not observational, i.e. due to the particular selection of the AGN sample, we deem that this effect is most likely physical and presumably due to the presence of absorption located in the large scale structure of the host galaxy. This extra absorption that we called for simplicity galactic, contributes to the total column density observed in X-rays and, even alone, could be sufficient to hide the broad line region providing a type 2 classification. The observed axial ratio distribution found in the present analysis can only be explained by considering a galactic absorption lying on the galaxy plane (e.g. inner bars, rings, dust lanes) in addition to the nuclear absorber. In this picture, the role played by the orientation of the two absorbing structures (large and small scale) is obviously more complicated than in the more conventional unified picture where only the orientation of the torus determines if a source is classified as a type 1 or 2. Within this scenario either absorber is capable of attenuating the BLR flux, and

so not only the orientation of each with respect to the line of sight is important but also their relative location and orientation. Following this scenario, when the torus and the galactic absorber are both edge-on, much of the absorbing material lies in the shadow of the torus leaving a wide range of angles which provide a direct view of the nucleus and therefore a type 1 classification. On the contrary, if the two absorbers are severely misaligned, then the absorbing material, either due to the torus or the galactic absorber, covers a much larger fraction of the nucleus, substantially increasing the probability that a randomly oriented observer will see a type 2 AGN. In this case we can have 3 configurations that provide a type 2 classification: one in which only the torus is detected, one where both absorbing structures lie along the line of sight and, finally, one where only a thick layer of galactic absorber is intercepted. In the first two cases the classification is that of a classical (torus hidden) type 2 AGN where the galactic absorption can eventually enhance the X-ray column density due to the torus. In the last case the source is formally not a type 2 AGN according to the classical unified theory, since the torus is not along the line of sight, but if $\text{Log}N_H > 21.6$ and the host galaxy is edge-on, the BLR becomes hidden and the source is optically classified as a type 2 AGN. In other words, if it were not for the host galaxy, these would be classified as type 1, i.e. it is the host galaxy that makes them appear as type 2. Given their relevance, it is important to find some examples of these AGN within our large data-set. If we assumed that the parsec scale tori are always Compton thick or nearly so, i.e. have column density above a few 10^{23} cm^{-2} , then objects with absorption much lower are probably hidden behind galactic material. Therefore in order to search for "misclassified" type 1 Seyferts, we focus on those Seyfert 1.8, 1.9 and 2 hosted in edge-on galaxies (i.e. having b/a below 0.5) and have mild X-ray absorption (below 10^{23} cm^{-2}), i.e. those located in the dashed region of figure 4. There are 22 such objects in our sample of INTEGRAL AGN, most of which are newly discovered and therefore poorly studied. For 9 of them broad band information could be gathered and analysed to verify their classification. These objects are shown in Table 1 where we list their name, presence of bar or dust lanes as reported in the literature and evidence, from the near infrared spectroscopy (NIR), for the presence of broad emission lines. The NIR regime is particularly useful from this purpose since, being less affected by dust extinction, is more likely to show a BLR otherwise hidden in the optical band. The sources listed in Table 1 are clear examples of how a type 1 nucleus can hide behind absorbing structures that are located in the host galaxy. Some objects like NGC 7172 (Smajić et al. 2012), NGC 2992 (Trippe et al. 2008), NGC 5252 (Kotilainen & Prieto 1995) and NGC 5506 (Nagar et al. 2002) have already been discussed in the literature as examples of how a Seyfert 1 can be disguised as a Seyfert 2 due to galactic obscuration, while the other examples are suggested here for the first time. Although with the available observations their number is small (these objects represent 40% of the sample) and not yet sufficient to compensate for the lack of type 1 AGN in edge-on galaxies, their existence indicates this kind of "misclassification" due to galactic absorption can take place and, if extended to a large number of objects, might explain the difference in the axial ratio distributions of type 1 and 2 AGN. On the other hand the existence of such objects gives support to the idea that an absorption

located at larger scales is at work within a large fraction of local AGN.

As said, now that the co-evolution of galaxies and black holes is well established (e.g. see Heckman & Best (2014) and references therein) and the advent of the ALMA observations probe and image the gas within 100 pc of the AGN, there is beginning to accumulate evidence of multi absorption components. Mass and gas concentrations in host galaxies which are responsible for the feeding mechanism in AGN, can also contribute to the obscuration of their nuclei. The mechanism appears to be that of kinematically decoupled embedded bars, i.e. the combination of a slowly rotating kpc-scale stellar bar and a kinematically decoupled nuclear bar, with overlapping dynamical resonances (Combes et al. 2013). Such resonances and kinematic decoupling are fostered by a large central mass concentration and high gas fraction. The gas is first halted in a nuclear ring (a few 100 pc scale), and then driven inward under the influence of the decoupled nuclear bar obscuring the central engine. This has been observed in ESO 428-G14, where the measured kinematics is consistent with a nuclear inflow, or inner bar, which feeds the AGN (Feruglio et al. 2020). Therefore the picture emerging from recent observations is that this galactic absorption may reside in different structures present in the host galaxy which include dust lanes, bars, rings etc. In this paper we focus on their contribution to the obscuration of the direct radiation from the AGN especially when the host galaxy is seen edge-on. With this in mind also Compton thick AGN could be explained as sources in which the two absorbers on galactic and nuclear scales are both aligned and seen edge on. A similar result was also obtained by Goulding et al. (2012), studying the deep silicate absorption features seen in many Compton-thick AGN. Goulding et al. (2012) found that an important contribution to the observed mid-IR extinction in these objects is dust located in the host galaxy, i.e. due to disturbed morphologies, dust lanes or galaxy inclination angles. However, these authors considered these two absorbers, galactic versus torus, as two alternative absorbing structures while here we assume that they could be both present in the same object and possibly aligned to enhance the nuclear obscuration. To produce Compton thick absorption our line of sight intercepts an edge-on torus and the galactic absorber (like for example an inner bar) can intervene or not depending if it is present or not in the host galaxy. The other possible geometry, i.e. that of a face on torus, either aligned or not with the galactic absorber, will always produce a Compton thin source (Buchner et al. 2019). Therefore we can say that a Compton thick AGN can have two flavours: one in which our line of sight intercepts only the torus and one in which both the torus and the galactic structure are seen edge-on. This last configuration produces objects like ESO 428-G14 and those discussed by Goulding et al. (2012). We note that the deep silicate absorption features observed in Goulding et al. (2012) sample, cannot be explained in terms of torus absorption models (see for example García-González et al. (2017)) and can only be produced by dust on galactic scales.

7. Summary and Conclusions

Using the hard X-ray selected sample of AGN detected by INTEGRAL/IBIS, in this work we have investigated the possible contribution of absorbing material located on a

scale of hundreds of parsecs, i.e. in the host galaxies, to the total amount of N_H measured in the X-ray band. By collecting the axial ratios (b/a) of the host galaxies for all our sample sources, we have verified that also within our hard X-ray selection sample there is a deficiency of around 24% ($\pm 5\%$) of type 1 AGN hosted in edge-on galaxies (those with $b/a < 0.5$). We have investigated the distribution of the host galaxies axial ratios in type 1 and type 2 AGN and further highlighted the optical Seyfert subclasses (type 1.5 for the unabsorbed and type 1.8 and 1.9 for absorbed AGN) to check whether there is a trend of the optical class with the inclination of the galaxy, in other words, we checked for the presence of absorption able to hide the BLR, or part of it, in the different galaxy axial ratios, and we found none. Possible bias in redshift has been excluded. We found the same effect in a well determined range of z ($0.026 < z < 0.095$) where the number and the distributions of the two classes are statistically the same (at 99.9% confidence). Clearly this indicates that some material located in the host galaxy on scales of hundreds of parsec and not aligned with the putative absorbing torus of the AGN can contribute to the column density measured in the X-ray band. In particular we have developed a scheme of the expected AGN type as a function of X-ray absorption and axial ratio in the different configuration of torus and galaxy inclinations: when the torus is seen edge-on, we always have a type 2 absorbed AGN independently of the host galaxy orientation; when the torus is seen face-on we may have a type 1 AGN unabsorbed or mildly absorbed or "misclassified type 2 objects where the absorption is on galactic scales. Plotting the axial ratio versus the column density for type 1 and type 2 we have highlighted peculiar sources and in particular have been able to identify a set of possible "misclassified type 2 AGN", i.e those which are absorbed (type 2) and located in edge-on galaxies. Our conclusion is that these absorptions, galactic versus torus, are not alternative but could be both present in the same object and possibly aligned to enhance the nuclear obscuration. Within this scenario a Compton thick AGN can come in two flavours: one in which our line of sight intercepts only the torus and one in which both the torus and the galactic structure are seen edge-on.

Acknowledgements

The authors acknowledge financial support from ASI under contract n. 2019-35-HH.0. We acknowledge the usage of the HyperLeda database (<http://leda.univ-lyon1.fr>). This research has made use of the NASA/IPAC Extragalactic Database (NED) and NASA/ IPAC Infrared Science Archive, which are operated by the Jet Propulsion Laboratory, California Institute of Technology, under contract with the National Aeronautics and Space Administration. Acknowledgements go to Rick White at Pan-STARRS database for his help in finding/interpreting PS1 tables. We thank Chiara Feruglio for worthwhile discussion. The authors also thank Marco Mignoli for useful discussion on AGN/host galaxy characteristics in optical/IR band, Eliana Palazzi and Andrea Rossi for imaging analysis in optical/IR band.

We thank the anonymous referee for useful remarks which helped us to improve the quality of this paper.

Table 1. Possible Misclassified type 1.9/2 AGN

name	dust [†] /bar	ref	NIR	BLR	ref
IGR J02343+3229= NGC 973	DC/N	1	—	—	—
IGR J09025-6814=UGC11397	—/Y	—	—	—	—
NGC 2992	DC/N	2	Y	3	—
NGC 5506	D-S/Y	4	Y	5	—
NGC 5252	R-I/N	2	Y	5	—
IGR J19039+3344=NGC2788A	D/Y	6	—	—	—
NGC 7172	DC/N	2	Y	7	—
NGC 7314	DC/Y	2	Y	5, 3	—
IGR J22367-1231=MKN 915	DC/N	2	Y	5	—

(†) Same nomenclature as used by Malkan et al. (1998). Ref: (1) Verstappen et al. 2013; (2) Malkan et al. 1998; (3) Onori et al. 2016; (4) Martini et al. 2003; (5) Lamperti et al. 2017; (6) NED; (7) Smajic et al. 2012.

References

- Antonucci, R. 1993, Annual Review of Astronomy and Astrophysics, 31, 473
- Bianchi, S., Antonucci, R., Capetti, A., et al. 2019, MNRAS, 488, L1
- Bianchi, S., Maiolino, R., & Risaliti, G. 2012, Advances in Astronomy, 2012, 1
- Bird, A. J., Bazzano, A., Malizia, A., et al. 2016, The Astrophysical Journal Supplement Series, 223, 15
- Brightman, M. & Nandra, K. 2011, Monthly Notices of the Royal Astronomical Society, 413, 1206
- Buchner, J., Brightman, M., Nandra, K., Nikutta, R., & Bauer, F. E. 2019, arXiv e-prints, arXiv:1907.13137
- Cappi, M., Panessa, F., Bassani, L., et al. 2006, A&A, 446, 459
- Chambers, K. C., Magnier, E. A., Metcalfe, N., et al. 2016, arXiv e-prints, arXiv:1612.05560
- Combes, F., García-Burillo, S., Audibert, A., et al. 2019, A&A, 623, A79
- Combes, F., García-Burillo, S., Casasola, V., et al. 2013, Astronomy & Astrophysics, 558, A124
- De Rosa, A., Panessa, F., Bassani, L., et al. 2012, Monthly Notices of the Royal Astronomical Society, 420, 2087
- de Vaucouleurs, G. 1959, Handbuch der Physik, 53, 275
- Di Gesu, L., Costantini, E., Piconcelli, E., et al. 2014, Astronomy & Astrophysics, 563, A95
- Elitzur, M. 2008, New Astronomy Reviews, 52, 274
- Ferruit, P., Wilson, A. S., & Mulchaey, J. 2000, The Astrophysical Journal Supplement Series, 128, 139
- Feruglio, C., Fabbiano, G., Bischetti, M., et al. 2020, ApJ, 890, 29
- García-Burillo, S., Combes, F., Schinnerer, E., Boone, F., & Hunt, L. K. 2005, Astronomy & Astrophysics, 441, 1011
- García-Burillo, S., Combes, F., Usero, A., et al. 2014, Astronomy & Astrophysics, 567, A125
- García-González, J., Alonso-Herrero, A., Höning, S. F., et al. 2017, Monthly Notices of the Royal Astronomical Society, 470, 2578
- Gelbord, J. M., Weaver, K. A., & Yaqoob, T. 2006, in ESA Special Publication, Vol. 604, The X-ray Universe 2005, ed. A. Wilson, 619
- González-Martín, O., Masegosa, J., Márquez, I., Guerrero, M. A., & Dultzin-Hacyan, D. 2006, Astronomy & Astrophysics, 460, 45
- Goulding, A. D., Alexander, D. M., Bauer, F. E., et al. 2012, The Astrophysical Journal, 755, 5
- Heckman, T. M. & Best, P. N. 2014, ARA&A, 52, 589
- Hickox, R. C. & Alexander, D. M. 2018, ARA&A, 56, 625
- Hirashita, H. & Nozawa, T. 2017, Planetary and Space Science, 149, 45
- Höning, S. F. 2019, ApJ, 884, 171
- Höning, S. F. & Kishimoto, M. 2017, ApJ, 838, L20
- Hubble, E. P. 1926, The Astrophysical Journal, 64, 321
- Huchra, J. P., Macri, L. M., Masters, K. L., et al. 2012, The Astrophysical Journal Supplement Series, 199, 26
- Jarrett, T. H., Chester, T., Cutri, R., Schneider, S. E., & Huchra, J. P. 2003, AJ, 125, 525
- Keel, W. C. 1980, The Astronomical Journal, 85, 198
- Kocevski, D. D., Brightman, M., Nandra, K., et al. 2015, The Astrophysical Journal, 814, 104
- Koss, M., Mushotzky, R., Veilleux, S., & Winter, L. 2010, The Astrophysical Journal, 716, L125
- Kotilainen, J. K. & Prieto, M. A. 1995, A&A, 295, 646
- Krivonos, R. A., Tsygankov, S. S., Mereminskiy, I. A., et al. 2017, Monthly Notices of the Royal Astronomical Society, 470, 512
- Lagos, C. d. P., Padilla, N. D., Strauss, M. A., Cora, S. A., & Hao, L. 2011, Monthly Notices of the Royal Astronomical Society, 414, 2148
- Lamperti, I., Koss, M., Trakhtenbrot, B., et al. 2017, Monthly Notices of the Royal Astronomical Society, stx055
- Madrid, J. P., Chiaberge, M., Floyd, D., et al. 2006, The Astrophysical Journal Supplement Series, 164, 307
- Maia, M. A. G., Machado, R. S., & Willmer, C. N. A. 2003, Bulletin of the Astronomical Society of Brazil, 23, 156
- Maiolino, R. & Rieke, G. H. 1995, The Astrophysical Journal, 454, 95
- Maiolino, R., Risaliti, G., & Salvati, M. 1999, A&A, 341, L35
- Makarov, D., Prugniel, P., Terekhova, N., Courtois, H., & Vauglin, I. 2014, Astronomy & Astrophysics, 570, A13
- Malizia, A., Bassani, L., Bazzano, A., et al. 2012, Monthly Notices of the Royal Astronomical Society, 426, 1750
- Malizia, A., Landi, R., Bassani, L., et al. 2007, The Astrophysical Journal, 668, 81
- Malizia, A., Landi, R., Molina, M., et al. 2016, Monthly Notices of the Royal Astronomical Society, 460, 19
- Malizia, A., Stephen, J. B., Bassani, L., et al. 2009, MNRAS, 399, 944
- Malkan, M. A., Gorjian, V., & Tam, R. 1998, The Astrophysical Journal Supplement Series, 117, 25
- Martini, P., Regan, M. W., Mulchaey, J. S., & Pogge, R. W. 2003, The Astrophysical Journal Supplement Series, 146, 353
- Mateos, S., Carrera, F. J., Alonso-Herrero, A., et al. 2016, The Astrophysical Journal, 819, 166
- Matt, G. 2000, A&A, 355, L31
- McKernan, B., Ford, K. E. S., & Reynolds, C. S. 2010, Monthly Notices of the Royal Astronomical Society, 407, 2399
- Mereminskiy, I. A., Krivonos, R. A., Lutovinov, A. A., et al. 2016, MNRAS, 459, 140
- Miniutti, G., Piconcelli, E., Bianchi, S., Vignali, C., & Bozzo, E. 2010, Monthly Notices of the Royal Astronomical Society, 401, 1315
- Molina, M., Bassani, L., Malizia, A., et al. 2013, Monthly Notices of the Royal Astronomical Society, 433, 1687
- Nagar, N. M., Oliva, E., Marconi, A., & Maiolino, R. 2002, Astronomy & Astrophysics, 391, L21
- Oda, S., Tanimoto, A., Ueda, Y., et al. 2017, The Astrophysical Journal, 835, 179
- Onori, F., La Franca, F., Ricci, F., et al. 2016, Monthly Notices of the Royal Astronomical Society, 464, 1783
- Panessa, F. & Bassani, L. 2002, A&A, 394, 435
- Panessa, F., Bassani, L., Landi, R., et al. 2016, Monthly Notices of the Royal Astronomical Society, 461, 3153
- Patrick, A. R., Reeves, J. N., Porquet, D., et al. 2012, Monthly Notices of the Royal Astronomical Society, 426, 2522
- Prieto, M. A., Mezcua, M., Fernández-Ontiveros, J. A., & Schartmann, M. 2014, Monthly Notices of the Royal Astronomical Society, 442, 2145
- Ricci, C., Beckmann, V., Audard, M., & Courvoisier, T. J.-L. 2010, Astronomy and Astrophysics, 518, A47
- Ricci, C., Trakhtenbrot, B., Koss, M. J., et al. 2017, The Astrophysical Journal Supplement Series, 233, 17
- Sazonov, S., Churazov, E., & Krivonos, R. 2015, MNRAS, 454, 1202
- Schinnerer, E., Eckart, A., & Tacconi, L. J. 1999, The Astrophysical Journal, 524, L5

- Simcoe, R., McLeod, K. K., Schachter, J., & Elvis, M. 1997, The Astrophysical Journal, 489, 615
- Smajić, S., Fischer, S., Zuther, J., & Eckart, A. 2012, Astronomy & Astrophysics, 544, A105
- Steenbrugge, K. C., Kaastra, J. S., Sako, M., et al. 2005, Astronomy & Astrophysics, 432, 453
- Trippe, M. L., Crenshaw, D. M., Deo, R., & Dietrich, M. 2008, The Astronomical Journal, 135, 2048
- Trippe, M. L., Crenshaw, D. M., Deo, R. P., et al. 2010, The Astrophysical Journal, 725, 1749
- Tsvetanov, Z., Caganoff, S., Kriss, G. A., et al. 1992, in Bulletin of the American Astronomical Society, Vol. 24, American Astronomical Society Meeting Abstracts #180, 752
- Urry, C. M. & Padovani, P. 1995, Publications of the Astronomical Society of the Pacific, 107, 803
- Ursini, F., Bassani, L., Panessa, F., et al. 2017, Monthly Notices of the Royal Astronomical Society, 474, 5684
- van der Laan, T. P. R., Armus, L., Beirao, P., et al. 2015, Astronomy & Astrophysics, 575, A83
- Vasudevan, R. V., Brandt, W. N., Mushotzky, R. F., et al. 2013, The Astrophysical Journal, 763, 111
- Verstappen, J., Fritz, J., Baes, M., et al. 2013, Astronomy & Astrophysics, 556, A54
- Winter, L. M., Mushotzky, R. F., Reynolds, C. S., & Tueller, J. 2009, ApJ, 690, 1322

Appendix A: New INTEGRAL AGN

Here we discuss the new AGN reported by Mereminskiy et al. (2016) in deep extragalactic surveys and those reported by Krivonos et al. (2017) from an extensive galactic plane mapping. Among the 147 sources reported by Mereminskiy et al. (2016), 70 are new hard X-ray emitting objects never reported in previous INTEGRAL surveys (Bird et al. 2016 and references therein): 23 of these are still unidentified and therefore have not been considered. Of the remaining 47 objects, all optically classified as AGN, 8 are blazars and 7 have no X-ray observation available to characterised their 2-10 keV spectra; they have therefore been excluded from the list of AGN considered in this work. The remaining 33 objects have instead been added to the large database of INTEGRAL AGN (Malizia et al. 2012, 2016). Regarding instead the new hard X-ray sources reported along the Galactic Plane Survey by Krivonos et al. (2017), 21 are identified with AGN by the authors: 11 are unambiguously classified as Seyfert galaxies and therefore have been added to the INTGRAL AGN sample, while the rest, being either blazars or objects of unknown class, have been omitted. All these new entries ($33 + 11$) have been listed in table A.2 and A.3 together with their coordinates, redshift, optical class and X-ray spectral parameters (column density, photon index, 2-10 and 20-100 keV fluxes) for uniformity with the work of Malizia et al. (2012, 2016). It is worth noting that also these new addition have been unambiguously associated with their X-ray counterparts thus allowing to restrict their positional error box and therefore to be optically identified and classified with good confidence. To provide the X-ray spectral parameters for these new 44 AGN, we have checked both the literature and the archives to search for information. In many cases, the X-ray data analysis has already been performed and the results reported in various publications as listed in the last column of Table A.2 and A.3. For 7 objects the X-ray data analysis is performed and presented here using archival Swift/XRT observations; in a couple of cases we preferred to re-analyse the data since more exposure or not convincing results were found (e.g. IGR J21099+3533 and IGR J21382+3204 already analysed by Ricci et al. 2017). The 2-10 keV spectral analysis has been performed following the method described in Malizia et al. (2016); the 20-100 keV fluxes have been converted from the 17-60 keV flux reported in Mereminskiy et al. (2016) and Krivonos et al. (2017) by assuming a simple power law $\Gamma=2.01\pm0.04$, as found by Molina et al. (2013).

Table A.1. INTEGRAL/IBIS AGN

Name	<i>z</i>	Class	Log N_H	b/a	Morph/BAR
IGR J00040+7020	0.0960	Sy2	22.52	1.00	–
IGR J00256+6821	0.0120	Sy2	23.60	0.62	–
IGR J00333+6122	0.1050	Sy1.5	21.93	1.00	–
SWIFT J0034.5-7904	0.0740	Sy1	20.79	0.74	–
IGR J00465-4005	0.2010	Sy2	23.38	–	–
Mrk 348	0.0153	Sy2	23.02	0.90	SA
Mrk 352	0.0150	Sy1	20.72	0.92	S0A
Mrk 1152	0.0537	Sy1.5	20.23	0.62	S
Firall 9	0.0470	Sy1.2	20.50	0.96	S0
NGC 526A	0.0191	Sy1.9	22.23	0.82	S0A
ESO 297-18	0.0252	Sy2	23.66	0.34	S
IGR J01528-0845	0.0370	Sy2	23.49	0.54	SB
IGR J01528-0326	0.0172	Sy2	23.15	0.16	SA
IGR J01545+6437	0.0349	Sy2	<21.82	0.62	–
Mrk 584	0.0788	Sy1.8	20.47	0.92	–
NGC 788	0.0136	Sy2	23.48	0.82	S0A
Mrk 1018	0.0424	Sy1	20.41	0.62	S0
IGR J02086-1742	0.1290	Sy1.2	<20.33	–	–
IGR J02097+5222	0.0492	Sy1	21.23	–	–
Mrk 590	0.0264	Sy1	20.42	0.94	SA
SWIFT J0216.3+5128	0.4220	Sy2?	22.10	0.74	–
Mrk 1040	0.0166	Sy1.5	20.56	0.34	SA
IGR J02343+3229	0.0162	Sy2/LINER	22.34	0.22	SA
NGC 985	0.0431	Sy1.5	20.50	0.90	SB?
NGC 1052	0.0050	Sy2/LINER	23.30	0.76	E
RBS 345	0.0690	Sy1	20.72	0.84	–
NGC 1068	0.0038	Sy2	>25.00	0.88	SB
QSO B0241+62	0.0445	Sy1.2	21.32	–	–
MCG -07-06-018	0.0696	XBONG	>24.00	0.56	S0A
SWIFT J0249.1+2627	0.0580	Sy2	23.43	0.70	–
IGR J02504+5443	0.0151	Sy2	24.20	0.28	S0
MCG -02-08-014	0.0167	Sy2?	23.08	0.22	S
NGC 1142	0.0288	Sy2	23.80	0.44	E
MCG -02-08-038	0.0326	Sy1	21.56	0.56	SAB
NGC 1194	0.0136	Sy2	24.20	0.58	S0A
PKS 0312-770	0.2252	Sy1/QSO	20.93	–	–
B3 B0309+411B	0.1340	Sy1	21.11	0.84	–
SWIFT J0318.7+6828	0.0901	Sy1.9	22.61	0.70	–
NGC 1275	0.0175	Sy1.5/LINER	21.08	0.83	S0
1H 0323+342	0.0610	NLS1	21.16	0.88	–
IGR J03249+4041-SW	0.0477	Sy2	21.18	0.76	–
IGR J03249+4041-NE	0.0475	Sy2	22.48	0.60	S
IGR J03334+3718	0.0558	Sy1.5	21.15	0.94	–
NGC 1365	0.0054	Sy1.9	24.65	0.82	SB
ESO 548-G81	0.0145	Sy1	20.36	0.42	SB
SWIFT J0353.7+3711	0.0186	Sy2/LINER	22.57	0.68	S0
4C +62.08	1.1090	Sy1	21.51	–	–
SWIFT J0357.6+4153	0.0530	Sy1.9	22.30	0.40	–
3C 098	0.0304	Sy2	23.08	0.92	E
4C 03.8	0.0890	Sy2	23.45	1.00	E
3C 111	0.0485	Sy1	21.66	0.80	E
IGR J04221+4856	0.1140	Sy1	21.85	–	–
LEDA 15023	0.0450	Sy2	23.48	0.72	E
3C120	0.0330	Sy1.5	21.20	0.64	S0
UGC 3142	0.0216	Sy1	22.60	0.78	S0B
SWIFT J0444.1+2813	0.0113	Sy2	22.53	0.62	S
SWIFT J0450.7-5813	0.0907	Sy1.5	20.80	0.68	–
MCG -01-13-025	0.0159	Sy1.2	20.55	0.90	SAB
LEDA 168563	0.0290	Sy1	21.73	0.72	–
SWIFT J0453.4+0404	0.0296	Sy2	24.16	0.68	E/S0A
ESO 033-G02	0.0181	Sy2	22.10	0.82	S0B
LEDA 075258	0.0160	Sy1	19.75	0.76	E

Name	<i>z</i>	Class	Log N _H	b/a	Morph/BAT
SWIFT J0505.8-2348	0.0350	Sy2	23.50	0.90	–
IGR J05081+1722	0.0175	Sy2	22.38	0.66	S0
4U 0517+17	0.0179	Sy1.5	20.95	–	E/S0
SWIFT J0515.3+1854	0.0235	Sy2	23.06	0.82	E
Ark 120	0.0327	Sy1	20.99	0.82	SA
SWIFT J0516.3+1928	0.0211	Sy2	22.64	0.26	S
SWIFT J0519.5-3140	0.0126	Sy1.5	21.90	0.76	S0B
PICTOR A	0.0351	Sy1/LINER	20.78	0.68	S0A
PKS 0521-36	0.0565	Sy1	20.55	–	S0
SWIFT J0544.4+5909	0.0659	Sy1.9	22.26	0.64	–
IGR J05470+5034	0.0360	Sy2	23.18	0.66	S0
NGC 2110	0.0078	Sy2	22.46	0.82	S0AB
MCG+08-11-011	0.0205	Sy1.5	21.32	0.48	SB
4U 0557-385	0.0339	Sy1.2	22.10	0.54	S0
IRAS 05589+2828	0.0330	Sy1	21.66	–	–
SWIFT J0601.9-8636	0.0064	Sy2	24.00	0.22	S
IGR J06058-2755	0.0900	Sy1.5	20.38	0.70	–
Mrk 3	0.0135	Sy2	24.00	0.82	SAB?
IGR J06233-6436	0.1289	Sy1	20.59	0.76	–
IGR J06239-6052	0.0405	Sy2	23.35	0.66	S0B
SWIFT J0623.8-3215	0.0224	Sy2	23.91	0.70	S0B
SWIFT J0640.4-2554	0.0248	Sy1.2	21.38	0.60	S
IGR J06415+3251	0.0172	Sy2	23.20	0.80	E
Mrk 6	0.0188	Sy1.5	22.90	0.70	S0AB
Mrk 79	0.2219	Sy1.2	20.72	0.60	SB
IGR J07565-4139	0.0210	Sy2	21.86	0.64	–
IGR J07597-3842	0.0400	Sy1.2	21.78	–	–
ESO 209-12	0.0405	Sy1.5	21.38	0.40	S
Mrk 1210	0.0135	Sy 2	23.52	0.88	S
PG 0804+761	0.1000	Sy1	20.70	–	E
IGR J08190-3835	0.0090	Sy2	23.13	0.94	–
FRL 1146	0.0316	Sy1.5	21.45	0.74	S
SWIFT J0845.0-3531	0.1370	Sy1.2	22.38	–	–
IGR J08557+6420	0.0370	Sy2?	23.29	0.40	S?
IGR J08558+0814	0.2200	Sy1	20.67	–	–
Mrk 18	0.0111	Sy2	23.26	0.46	S0
IGR J09025-6814	0.0140	XBONG	22.90	0.32	SAB
IGR J09026-4812	0.0391	Sy1	21.98	0.56	–
1RXS J090431.1-382920	0.0160	Sy1	21.46	0.54	S
SWIFT J0917.2-6221	0.0573	Sy1	21.61	0.44	–
IGR J09189-4418	–	AGN	22.66	0.84	–
MCG-01-24-012	0.0196	Sy2	22.80	0.78	SAB
Mrk 110	0.0353	NLS1	20.30	0.92	E
IGR J09253+6929	0.0390	Sy1.5	23.15	0.74	–
SWIFT J0929.7+6232	0.0256	Sy2	23.31	0.96	E
IGR J09446-2636	0.1425	Sy1.5	20.81	0.38	–
NGC 2992	0.0077	Sy2	21.90	0.45	SA
MCG-05-23-016	0.0085	Sy2	22.21	0.60	S0
4C 73.08	0.0581	Sy2	23.96	0.90	–
IGR J09523-6231	0.2520	Sy1.9	22.80	–	–
M81	0.0008	Sy1.8/LINER	20.74	0.52	SA
NGC 3081	0.0079	Sy2	23.82	0.68	SAB
SWIFT J0959.7-3112	0.0370	Sy1	20.80	0.58	S0B
NGC 3079	0.0037	Sy2	24.00	0.26	SB
SWIFT J1009.3-4250	0.0330	Sy2	23.41	0.82	SAB
IGR J10147-6354	0.2020	Sy1.2	22.30	–	–
NGC 3227	0.0038	Sy1.5	22.83	0.57	SAB
NGC 3281	0.0107	Sy2	24.18	0.44	SAB
SWIFT J1038.8-4942	0.0600	Sy1.5	21.79	0.80	–
IGR J10404-4625	0.0240	Sy2	22.61	0.66	S0
MCG+04-26-006	0.0200	LINER	23.09	0.74	SA

Name	<i>z</i>	Class	Log N _H	b/a	Morph/BAT
NGC 3516	0.0088	Sy1.5	22.50	0.88	S0B
IGR J11366-6002	0.0140	Sy2/LINER	22.40	0.46	—
NGC 3783	0.0097	Sy1.5	22.06	0.94	SB
SWIFT J1143.7+7942	0.0065	Sy1.2	20.00	0.64	S0B
H1143-182	0.0329	Sy1.5	20.48	0.68	SA
PKS 1143-696	0.2440	Sy1.2	21.21	—	—
B2 1144+35B	0.0631	Sy1.9	20.23	0.66	—
SWIFT J1200.8+0650	0.0360	Sy2	22.92	0.56	S0
IGR J12026-5349	0.0280	Sy2	22.41	0.78	S0B
NGC 4051	0.0023	NLS1	<21.48	0.60	SAB
NGC 4074	0.0224	Sy2	23.48	0.60	S0
Mrk 198	0.0242	Sy2	23.00	0.74	S0AB
NGC 4138	0.0030	Sy1.9	22.95	0.66	S0A
NGC 4151	0.0033	Sy1.5	23.34	0.59	SAB
IGR J12107+3822	0.0229	Sy1.5	22.67	0.82	E
IGR J12131+0700	0.2095	Sy1.5-1.8	20.14	—	—
NGC4235	0.0080	Sy1.2	21.20	0.28	SA
Mrk 766	0.0129	NLS1	<21.95	0.84	SB
NGC 4258	0.0015	Sy2	23.03	0.49	SAB
PKS 1217+02	0.2402	Sy1.2	20.25	—	—
Mrk 50	0.0234	Sy1	<21.08	0.86	S0
NGC 4388	0.0084	Sy2	23.44	0.33	SAB
NGC 4395	0.0011	Sy2	22.72	0.63	SB
3C 273	0.1583	Sy1/QSO	20.23	1.00	—
Mrk 771	0.0630	Sy1	20.88	0.82	S0B
XSS J12303-4232	0.1000	Sy1.5	20.88	—	—
NGC 4507	0.0118	Sy2	23.64	0.84	SAB
SWIFT J1238.6+0928	0.0829	Sy2	23.52	0.68	S0
ESO 506-G27	0.0250	Sy2	23.03	0.44	S0
LEDA 170194	0.0367	Sy2	22.46	0.88	S0
NGC 4593	0.0090	Sy1	20.30	0.54	SB
IGR J12415-5750	0.0242	Sy1.5	21.48	0.74	S
IGR J12482-5828	0.0280	Sy1.9	22.35	0.60	—
NGC 4748	0.0146	NLS1	20.56	0.72	SA
ESO 323-32	0.0160	Sy2	25.00	0.74	S0B
Mrk 783	0.0672	NLS1	21.80	1.00	E
IGR J13038+5348	0.0300	Sy1.2	20.22	0.56	—
NGC 4941	0.0037	Sy2	23.64	0.53	SAB
IGR J13042-1020	0.0104	Sy2	>25.00	0.71	SA
NGC 4945	0.0019	Sy2	24.72	0.31	SB
ESO 323-77	0.0150	Sy1.2	21.57	0.84	SB
IGR J13091+1137	0.0291	XBONG	23.63	0.58	SB
IGR J13107-5626	—	AGN	23.59	0.50	—
IGR J13109-5552	0.104	Sy1	<21.66	—	—
IGR J13133-1109	0.0343	Sy1	20.42	0.80	—
IGR J13149+4422	0.0353	Sy2/LINER	22.72	0.56	S0
IGR J13168-7157	0.0705	Sy1.5	21.21	0.74	—
NGC 5100	0.0319	LINER	23.16	—	S0
MCG-03-34-063	0.0213	Sy2	23.59	0.36	SB
Cen A	0.0018	Sy2	23.17	0.96	S0
ESO 383-18	0.0124	Sy2	23.29	0.50	S
MCG-06-30-015	0.0077	Sy1.2	22.17	0.54	S
NGC 5252	0.0230	Sy1.9	22.83	0.50	S0
IGR J13415+3033	0.0398	Sy2	23.47	0.62	SB
SWIFT J1344.7+1934	0.0271	Sy2/LINER	23.39	0.38	S0
IGR J13466+1921	0.0850	Sy1.2	20.27	0.82	S
Cen B	0.0129	RG/type2	22.11	0.80	E
4U 1344-60	0.0130	Sy1.5	23.67	—	S
IGR J13477-4210	0.0386	Sy2	22.79	0.72	—
IC 4329A	0.0160	Sy1.2	21.54	0.34	S0A
1AXG J135417-3746	0.0509	Sy1.9	22.80	0.78	—

Name	<i>z</i>	Class	Log N _H	b/a	Morph/BAR
IGR J13550-7218	0.0710	Sy2	23.28	—	—
PKS 1355-416	0.3130	Sy1	21.43	—	—
IGR J14080-3023	0.0237	Sy1.5	20.56	0.94	—
SWIFT J1410.9-4229	0.0339	Sy2	22.76	0.56	—
Circinus Galaxy	0.0014	Sy2	25.60	0.41	SA
NGC 5506	0.0062	Sy2	22.53	0.28	SAB
IGR J14175-4641	0.0760	Sy2	23.88	0.66	—
NGC 5548	0.0172	Sy1.5	20.19	0.86	S0A
ESO 511-G030	0.0224	Sy1	20.70	0.90	SA
H 1419+480	0.0723	Sy1.5	20.83	—	—
IGR J14301-4158	0.0039	Sy2	22.08	0.46	—
NGC 5643	0.0040	Sy2	23.85	0.98	SAB
NGC 5674	0.0249	Sy1.9	23.05	0.82	SAB
SWIFT J1436.8-1615	0.1445	Sy1/QSO	20.88	0.88	—
NGC 5728	0.0093	Sy2	24.14	0.44	SAB
IGR J14471-6414	0.0530	Sy1.2	21.60	—	—
IGR J14471-6319	0.0380	Sy2	23.39	—	—
IGR J14488-4008	0.1230	Sy1.2	22.89	—	—
IGR J14492-5535	—	AGN	23.08	—	—
IGR J14515-5542	0.0180	Sy2	21.52	0.50	S
PKS 1451-375	0.3140	Sy1.2	20.80	—	S0
IGR J14552-5133	0.0160	NLS1	21.53	0.80	S
IGR J14561-3738	0.0240	Sy2	>24.00	0.66	SB
IC 4518A	0.0163	Sy2	23.15	—	S
MKN 841	0.0364	Sy1.5	20.84	0.98	E
IRAS 15091-2107	0.0446	NLS1	21.15	0.78	S
SWIFT J1513.8-8125	0.0684	Sy1.2	21.88	0.60	—
ESO 328-36	0.0237	Sy1.8	20.84	—	S0
IGR J15301-3840	0.0155	Sy2	22.99	0.40	SA
IGR J15311-3737	0.1270	Sy1	21.32	—	—
MCG -01-40-001	0.0227	Sy2	22.59	0.34	S
IGR J15359-5750	—	AGN	23.30	—	—
IGR J15415-5029	0.0320	Sy2?	<22.04	0.52	S
NGC 5995	0.0252	Sy1.9	21.93	0.88	SAB
IGR J15539-6142	0.0150	Sy2	23.24	0.26	S
IGR J15549-3740	0.0190	Sy2	22.76	0.64	S
IGR J16024-6107	0.0110	Sy2	21.40	—	S
IGR J16056-6110	0.0520	Sy1.5	21.31	0.72	S
IGR J16058-7253(1)	0.0690	Sy2?	23.24	0.80	—
IGR J16058-7253(2)	0.0900	Sy2	23.58	0.52	—
IGR J16119-6036	0.0160	Sy1.5	21.36	0.96	SB
IGR J16185-5928	0.0350	NLS1	23.02	0.88	SAB
Mrk 1498	0.0547	Sy1.9	23.76	0.82	E
SWIFT J1630.5+3925	0.0306	Sy2	23.60	0.44	S0
IGR J16351-5806	0.0091	Sy2	24.68	0.87	SAB
IGR J16385-2057	0.0269	NLS1	21.08	0.80	E
IGR J16426+6536	0.3230	NLS1	20.41	—	—
IGR J16482-3036	0.0313	Sy1	21.00	0.72	—
SWIFT J1650.5+0434	0.0321	Sy2	22.68	0.74	E
ESO 138-1	0.0091	Sy2	>24.16	0.62	SAB
NGC 6221	0.0050	Sy2	22.04	0.74	SB
NGC 6240	0.0245	Sy2/LINER	24.30	0.56	S0
IGR J16558-5203	0.0540	Sy1.2	23.48	—	—
IGR J17009+3559	0.1130	XBONG	23.37	0.52	—
IGR J17036+3734	0.0650	Sy1	20.39	0.84	E
IGR J17111+3910	—	AGN	20.55	0.58	SB
NGC 6300	0.0037	Sy2	23.38	0.67	SB
MCG+08-31-041	0.0242	Sy1/LINER	<21.22	0.94	E
IGR J17204-3554	—	AGN	23.20	—	—
Mrk 506	0.0430	Sy1.5	<20.70	0.78	SAB
SWIFT J1723.5+3630	0.0400	Sy1.5	21.28	0.46	E

Name	<i>z</i>	Class	Log N _H	b/a	Morph/BAR
IGR J17348-2045	0.0440	Sy2	23.23	—	—
IGR J17379-5957	0.0170	Sy2	20.79	0.78	SA
GRS 1734-294	0.0214	Sy1	>21.32	—	—
2E 1739.1-1210	0.0370	Sy1.2	21.18	—	—
IGR J17476-2253	0.0463	Sy1	21.48	—	—
IGR J17488-2338	0.2400	Sy1.5	22.06	—	—
IGR J17488-3253	0.0200	Sy1	21.53	—	—
IGR J17513-2011	0.0470	Sy1.9	21.82	—	—
IGR J17520-6018	0.1120	Sy2	23.11	1.00	—
1RXS J175252.0-053210	0.1360	Sy1.2	21.33	—	—
NGC 6552	0.0265	Sy2	23.84	0.46	SB
IGR J18027-1455	0.0350	Sy1	21.48	—	—
IGR J18078+1123	0.0780	Sy1.2	22.25	0.92	—
IGR J18129-0649	0.7750	Sy1/QSO	21.54	—	—
SWIFT J1821.6+5953	0.0990	Sy2	22.88	1.00	—
IGR J18218+6421	0.2970	Sy1.2	20.54	—	—
IGR J18244-5622	0.0169	Sy2	23.15	0.38	SB
IGR J18249-3243	0.3550	Sy1/QSO	21.14	—	—
IGR J18259-0706	0.0370	Sy1	21.91	—	—
IGR J18308+0928	0.0190	Sy2	23.07	0.56	—
IGR J18311-3337	0.0687	Sy2	22.15	0.74	—
3C 382	0.0579	Sy1	20.79	0.68	E
Fairall 49	0.0200	Sy2	22.09	0.88	S
ESO 103-35	0.0133	Sy2	23.30	0.36	S0A
3C 390.3	0.0561	Sy1.5	20.63	0.84	E
ESO 140-43	0.0142	Sy1.5	23.04	0.44	SB
SWIFT J1845.4+7211	0.0463	Sy2	22.51	0.42	S
IGR J18470-7831	0.0743	Sy1	20.08	0.60	—
PBC J1850.7-1658	—	AGN	22.17	—	—
IGR J18538-0102	0.1450	Sy1	21.61	—	—
ESO 25-2	0.0292	Sy1	20.92	0.98	SB
2E 1853.7+1534	0.0840	Sy1	<21.59	0.92	—
2E 1849.2-7832	0.0420	Sy1	20.92	0.56	S0B
IGR J19077-3925	0.0760	Sy1.9	21.15	0.58	—
IGR J19118-1707	0.0234	LINER	23.02	0.72	S
PKS 1916-300	0.1668	Sy1.5-1.8	20.90	—	—
ESO 141-G055	0.0371	Sy1.2	20.68	0.82	S
SWIFT J1930.5+3414	0.0629	Sy1.5-1.8	23.44	—	—
SWIFT J1933.9+3258	0.05775	Sy1.2	<20.60	—	—
IGR J19378-0617	0.0106	NLS1	23.50	0.86	E
IGR J19405-3016	0.0520	Sy1.2	20.96	0.70	—
NGC 6814	0.0052	Sy1.5	21.10	0.94	SAB
XSS J19459+4508	0.0539	Sy2	23.04	0.56	—
IGR J19491-1035	0.0246	Sy1.2	22.26	0.82	E
3C 403	0.0590	Sy2	23.65	0.74	E
Cyg A	0.0561	Sy2	23.30	0.84	S
ESO 399-20	0.0249	NLS1	20.85	0.64	E
NGC 6860	0.0149	Sy1.5	21.00	0.64	SB
SWIFT J2018.4-5539	0.0606	Sy2	23.50	0.60	E
IGR J20186+4043	0.0144	Sy2	22.76	0.74	—
IGR J20216+4359	0.0170	Sy2	23.11	0.68	—
IGR J20286+2544(1)	0.0139	Sy2/SB	23.78	0.44	S
IGR J20286+2544(2)	0.0144	Sy2	23.97	0.40	S0A
NGC 6926	0.0196	Sy2	24.00	0.46	SB
4C +21.55	0.1735	Sy1	21.78	0.36	—
4C 74.26	0.1040	Sy1	21.15	—	—
SWIFT J2044.0+2832	0.0500	Sy1	21.24	—	—
Mrk 509	0.0344	Sy1.5	20.63	0.82	—
IGR J20450+7530	0.0950	Sy1	21.20	1.00	—
S52116+81	0.0840	Sy1	21.38	0.70	—
IGR J21178+5139	—	AGN	22.32	—	—

Name	<i>z</i>	Class	Log N _H	b/a	Morph/BAR
1RXS J211928.4+333259	0.0510	Sy1.5	21.52	—	—
IGR J21247+5058	0.0200	Sy1	22.89	—	—
SWIFT J2127.4+5654	0.0147	NLS1	21.90	—	—
CTS 109	0.0299	Sy1.2	20.55	0.80	S0
RX J2135.9+4728	0.0250	Sy1	20.30	—	—
1RXS J213944.3+595016	0.1140	Sy1.5	21.54	—	—
IGR J21565+5948	0.2080	Sy1	21.81	—	—
SWIFT J2156.2+1724	0.0340	Sy1.8	23.33	1.00	—
Mrk 520	0.0266	Sy1.9	22.63	—	S0
NGC 7172	0.0087	Sy2	22.86	0.50	SA
UGC 12040	0.0213	Sy1.9	< 22.92	0.66	S0B
IGR J22292+6647	0.1120	Sy1.5	21.68	—	—
NGC 7314	0.0048	Sy1.9	22.02	0.44	SAB
IGR J22367-1231	0.0241	Sy1.9	22.42	0.44	SA
3C 452	0.0811	Sy2	23.77	0.66	E
QSO B2251-178	0.0640	Sy1.2	22.33	0.84	S0
KAZ 320	0.0345	NLS1	20.68	0.72	S
NGC 7465	0.0066	Sy2/LINER	23.66	0.74	SB
NGC 7469	0.0163	Sy1.5	20.46	0.91	SAB
MCG-02-58-022	0.0469	Sy1.5	20.56	0.86	SA
NGC 7479	0.0079	Sy1.9	24.30	0.40	SB
NGC 7582	0.0052	Sy2	24.04	0.35	SB
IGR J23206+6431	0.0717	Sy1	21.95	0.70	—
RHS 61	0.1200	Sy1	20.59	1.00	—
IGR J23308+7120	0.037	Sy2 ?	22.96	0.92	—
IGR J23524+5842	0.164	Sy2 ?	22.46	—	—
IGR J23558-1047	1.1080	Sy1/QSO	20.41	—	—

Note: N_H values in bold are referring to upper limits or Galactic values.

Table A.2. INTEGRAL/IBIS AGN

Mereminsky												
Name	RA	dec	z	class	Log N _H	$\Gamma_{2-10 \text{ keV}}$	F _S [†]	F _H [‡]	b/a	Morph/BAR	Ref.	
SWIFT J0308.5-7251	03 07 35.32	-72 50 02.5	0.0276	Sy1.2	-	1.80±0.17	4.80	7.56	0.80	S	1	
SWIFT J0422.7-5611	04 22 24.18	-56 13 33.5	0.0435	Sy2	22.89	1.38±0.21	3.40	16.00	-	S	1	
1H0419-577 ^(a)	04 26 00.72	-57 12 01.0	0.1040	Sy1.5	19-22	1.70±0.01	8-16	22.34	-	-	2	
SWIFT J0440.2-5941	04 38 59.00	-59 40 54.0	0.0577	Sy2	22.34	2.12±0.27	2.80	7.74	0.38	-	1	
SWIFT J0504.6-7345	05 04 34.20	-73 49 27.1	0.0452	Sy1.9	21.91	1.78±0.15	3.40	8.44	0.62	-	1	
SWIFT J0505.6-6735	05 05 24.35	-67 34 35.4	0.046	likely Sy2	23.74	1.50±0.76	1.00	10.90	0.42	-	1	
IGR J05347-6015	05 34 30.90	-60 16 15.6	0.0570	Sy1	22.56	1.96±0.50	4.73	15.13	0.48	-	3	
SWIFT J0634.7-7445	06 34 03.52	-74 46 37.6	0.1120	Sy1	-	1.61±0.25	2.10	7.56	-	-	1	
IGR J06569-6534	06 56 29.20	-65 33 38.0	0.0295	Sy1	<22.23	1.77±0.50	1.70	9.00	0.78	S	3	
SWIFT J0747.6-7326	07 47 38.36	-73 25 53.2	0.0360	Sy2	23.56	1.40±0.53	1.30	12.31	0.92	E	1	
NGC 2655	08 55 37.73	+78 13 23.1	0.0047	LINER	23.36	1.9 (fixed)	1.05	7.56	0.90	SAB	4	
SWIFT J0935.9+6120	09 35 51.60	+61 21 11.4	0.0394	Sy2	24.12	1.63±0.20	0.20	5.10	0.70	S0	5	
SWIFT J1033.6+7303	10 34 23.54	+73 00 50.2	0.0220	XBONG	22.62	1.53±0.22	2.60	7.21	0.48	S0	1	
SWIFT J1044.1+7024	10 44 08.54	+70 24 19.3	0.0336	Sy2	23.27	1.58±0.35	2.20	8.97	0.36	S	1	
SWIFT J1105.7+5854 ^(b)	11 06 49.55	+57 41 07.7	0.0322	Sy2	23.87	2.20 (fixed)	0.66	11.78	0.60	S0	6	
SWIFT J1114.3+7944	11 14 43.91	+79 43 35.9	0.0372	Sy2	22.66	1.42±0.67	1.70	7.39	0.56	-	1	
SWIFT J1144.1+3652	11 44 29.88	+36 53 08.6	0.03801	Sy1	-	1.80±0.04	1.84	9.85	0.90	S	6	
SWIFT J1148.3+0901	11 47 55.08	+09 02 28.8	0.0688	Sy1.5	-	1.78±0.08	4.00	6.16	0.74	-	6	
SWIFT J1148.7+2941	11 48 45.95	+29 38 28.3	0.0230	LINER	22.70	1.51±0.81	5.15	12.66	0.48	S0	6	
SWIFT J1201.2-0341	12 01 14.36	-03 40 41.1	0.0196	Sy 1	-	1.98±0.15	6.10	10.20	0.80	E	1	
3PBC J1204.7+3109	12 04 43.32	+31 10 38.2	0.0250	Sy1.9	23.00	1.88±0.08	2.30	9.67	0.90	SB	6	
SWIFT J1207.5+3355	12 07 32.90	+33 52 40.0	0.0791	Sy2	22.70	1.50±0.13	1.60	7.74	0.68	E	1	
NGC 4180	12 13 03.05	+07 02 20.2	0.0070	LINER	24.16	1.92±0.12	0.20	23.39	0.38	SB	1	
WAS 49B	12 14 17.73	+29 31 43.2	0.0640	Sy2	23.41	2.03±0.33	2.60	9.85	0.96	-	1	
IGR J12171+7047	12 17 26.20	+70 48 07.2	0.0067	AGN	23.40	1.7 (fixed)	0.34	8.44	0.50	S0B	3	
MRK 205	12 21 44.22	+75 18 38.8	0.0708	Sy1	23.71	1.97±0.02	0.93	13.54	-	SB	7	
3PBC J1231.3+7044	12 31 36.44	+70 44 14.1	0.2080	Sy1.2	22.78	2.01±0.07	0.57	8.62	-	-	8	
NGC 4579	12 37 43.52	+11 49 05.5	0.0051	Sy1.9	-	1.78±0.1	3.91	8.79	0.95	SAB	3	
SWIFT J1240.9+2735	12 40 46.41	+27 33 53.7	0.0567	Sy2	22.45	1.23±0.45	2.10	8.79	0.78	S	1	
NGC 4736	12 50 53.06	+41 07 13.6	0.0010	Sy2/LINER	20.90	2.00±0.15	0.14	8.79	0.85	SA	9	
SWIFT J1300.1+1635	13 00 05.35	+16 32 14.9	0.0800	Sy2	22.5	1.50±0.17	2.04	6.16	0.78	-	5	
NGC 5033	13 13 27.47	+36 35 38.2	0.0029	Sy1.9	-	1.70±0.1	2.87	11.26	0.56	-	10	
3PBC J1342.0+3539	13 42 08.34	+35 39 15.2	0.0036	Sy1.9	21.95	1.40±0.1	6.71	17.76	0.84	S0A	10	

^(†): 2-10 keV flux in units of $10^{-12} \text{ erg cm}^{-2} \text{ s}^{-1}$ ^(‡): 20-100 keV flux in units of $10^{-12} \text{ erg cm}^{-2} \text{ s}^{-1}$

(a): highly variable source both in flux and spectral shape (see Di Gesù et al. 2014)

(b): blended source Sy2 (CGCG 291-028) and QSO, in table values referred to the Sy2 only (not included in the analysis)

References: (1): Ricci et al. 2017 ;(2): Di Gesu et al. 2014; (3): **this work**; (4): Brightman & Nandra 2011; (5): Oda et al. 2017; (6): Vasudevan et al. 2013; (7):Patrick et al. 2012; (8): Miniutti et al. 2010; (9): González-Martín et al. 2006; (10): Cappi et al. 2006;

Table A.3. INTEGRAL/IBIS AGN

Krivonos												
Name	RA	dec	z	class	Log N _H	Γ _{2–10 keV}	F [†] _S	F [†] _H	b/a	Morph/BAR	Ref.	
IGR J03117+5028	03 11 54.72	+50 30 21.1	0.0624	Sy1.5	21.08	1.80±0.16	5.9	8.64	0.56	–	1	
IGR J07396–3143	07 39 44.69	-31 43 02.5	0.0261	Sy2	23.46	1.41±0.31	1.0	21.35	0.48	S0	1	
IGR J07433–2544	07 43 14.72	-25 45 50.1	0.023	Sy1	20.95	2.08±0.20	9.5	15.05	0.84	–	1	
IGR J08398–1214	08 39 50.59	-12 14 34.3	0.198	Sy1	20.00	2.03±0.08	11.4	22.21	–	–	1	
IGR J16494–1740	16 49 21.02	-17 38 40.3	0.0229	Sy2	22.25	1.36±0.36	2.3	9.87	0.18	S	3	
IGR J19039+3344	19 03 49.16	+33 50 40.7	0.0150	Sy2	22.87	1.79±0.18	4.6	12.96	0.40	SB	1	
IGR J19260+4136	19 26 30.22	+41 33 04.9	0.0720	Sy2	20.49	1.71±0.08	5.5	8.14	0.52	–	1	
IGR J21099+3533	21 09 31.88	+35 32 57.6	0.2023	Sy1	21.10	2.11±0.07	3.5	8.76	0.62	–	3	
IGR J21382+3204	21 38 33.41	+32 05 06.1	0.0251	Sy1.5	22.44	1.82±0.35	2.5	15.67	0.56	S	3	
IGR J21397+5949	21 39 44.97	+59 50 15.0	0.114	Sy1.5	21.46	1.74±0.82	7.0	9.62	–	–	1	

(†): 2–10 keV flux in units of 10^{-12} erg cm $^{-2}$ s $^{-1}$;(‡): 20–100 keV flux in units of 10^{-12} erg cm $^{-2}$ s $^{-1}$

References as in Tab A1